Multi-Class Coded Layered Asymmetrically Clipped Optical OFDM

Xiaoyu Zhang, *Student Member, IEEE,* Zunaira Babar, *Member, IEEE,* Rong Zhang, *Senior Member, IEEE,* Sheng Chen, *Fellow, IEEE,* and Lajos Hanzo, *Fellow, IEEE*

***Abstract*—Multi-class channel coded layered asymmetrically clipped optical orthogonal frequency division multiplexing (LACO-OFDM) is proposed, where the achievable rate of the system is derived based on our mutual information analysis. We conceive a multi-class channel encoding scheme integrated with the layered transmitter. At the receiver both the coded and uncoded likelihood ratios (LLRs) are extracted for inter-layer interference cancellation and symbol detection, respectively. Simulations are conducted and the results show that our design approaches the achievable rate within 1.1 dB for 16QAM 4-layer LACO-OFDM with the aid of a half-rate 8-iteration turbo code at BER $= 10^{-3}$, outperforming its conventional counterpart by about 3.6 dB.**

***Index Terms*—Optical communications, forward error correction, layered asymmetrically clipped optical orthogonal frequency division multiplexing (LACO-OFDM), achievable rate.**

I. Introduction

Visible light communications (VLC) constitutes a promising optical wireless technique, which has been rapidly developed into a practical solution [1], [2]. Thanks to the popularity of energy-efficient light emitting diodes (LED) in indoor lighting systems, as an additional benefit, their ability to transmit information has also been explored [3], [4].

Photo diodes (PD) can be used as the VLC receiver relying on intensity modulation combined with direct detection (IM/DD) as a benefit of its low complexity. Explicitly, the intensity of the light ray is modulated with the information and the PD at the receiver detects this and converts it into electric signal for further processing [5]. The ubiquitous orthogonal frequency division multiplexing (OFDM) technique has also been transplanted from the radio frequency (RF) field into the VLC domain [6], [7]. During the transfiguration of RF-OFDM into optical OFDM (O-OFDM), a major impediment surfaced, because IM/DD requires real- and positive-valued signals to be mapped to the lightwave, but the complex-valued signal produced by the conventional RF-OFDM cannot satisfy this specification. Therefore, modifications have to be made, so that the unipolar requirement is met [8]. Hence numerous propositions can be found in the literature, which are surveyed below.

Specifically, the data to be transmitted may be mapped to the frequency domain (FD) representation of the O-OFDM signal by obeying the Hermitian symmetry, which is capable of guaranteeing pure real-valued time domain (TD) symbols after the inverse fast Fourier transform (IFFT) based modulation. This requires the first half of the FD symbols to be the conjugate of the rest, as detailed in [6]. The direct current (DC) based optical OFDM (DCO-OFDM) scheme was proposed by Carruthers and Kahn in [9] based on the Hermitian symmetry, where a sufficiently high DC offset is added to the real-valued signal so that all but the most negative parts become positive, whilst the remaining negative values are set to zero. DCO-OFDM is however energy-inefficient due to the typically 7 dB or higher DC shift [10], [11]. Armstrong and Lowery [12] later proposed the asymmetrically clipped optical OFDM (ACO-OFDM) philosophy, where every other subcarrier is left blank and additionally, the overall FD signal still has to satisfy Hermitian symmetry. Then the IFFT-based modulation provides a signal, where all the negative samples have a positive counterpart with the same magnitude, hence the negative samples can be discarded. Thus the original signal can still be recovered without information loss at the receiver side. However, the above-mentioned FD process leaves three quarters of the subcarriers with either zero or redundant conjugate symbols, which is spectrally inefficient. More specifically, comparing DCO-OFDM to ACO-OFDM, it is readily observed that the former is more spectral-efficient than the latter, while the latter is more energy-efficient than the former, which yields a design dilemma.

Against this background, Q. Wang *et al.* [13] proposed layered ACO-OFDM (LACO-OFDM), which offers a higher spectral efficiency than the classic ACO-OFDM, while maintaining moderate power efficiency. According to [13], LACO-OFDM embeds additional ACO-OFDM layers within the classic ACO-OFDM frame, which occupy the blank even-indexed ACO-OFDM subcarriers, hence, enhancing the spectral efficiency. However, this is achieved at the cost of inter-layer interference (ILI). Specifically, after re-modulation at the receiver, the negative clipping distortion of the lower layers falls on the subcarriers occupied by the upper layers, which constitutes the ILI. Nonetheless, the multiple ACO-OFDM layers within the LACO-OFDM frame can be detected sequentially using successive interference cancellation (SIC) [14], commencing from the first layer, which is free from ILI. Over the same time period, the spectral and energy

The European Research Council's Advanced Fellow Grant QuantCom and the EPSRC's financial supports are gratefully acknowledged.

The financial support of the RS GCRF, of the EPSRC projects EP/Noo4558/1, EP/PO34284/1 as well as of the European Research Council's Advanced Fellow Grant QuantCom is gratefully acknowledged.

The authors acknowledge the use of the IRIDIS High Performance Computing Facility, and associated support services at the University of Southampton, in the completion of this work.

The authors are with the School of Electronics and Computer Science, University of Southampton, Southampton, SO17 1BJ, U.K. (e-mail:{xz3u13,zb2g10,rz,sqc,lh}@ecs.soton.ac.uk).

efficient OFDM (SEE-OFDM) [15], [16] and enhanced ACO-OFDM (eACO-OFDM [17] and EACO-OFDM [18]) were independently proposed using similar philosophy.

Since the higher layers of a LACO-OFDM frame rely on the lower layers for estimating interference, any residual detection errors in the lower layers propagate through all the successive layers. Consequently, the higher layers exhibit a higher bit error ratio (BER) than the lowers layers [19]. As a further advance, Q. Wang *et al.* [20] also conceived an improved detection method, which exploits the TD signal for reducing the ILI. Another improved LACO-OFDM receiver relying on soft SIC was proposed by T. Wang *et al.* [21], which exploits the idea of diversity combining for eliminating ILI. Parallel to those developments, Mohammed *et al.* [22] studied both FD and TD diversity combining conceived for LACO-OFDM systems.

Against this background, in this paper we conceive an integrated multi-class forward error correction (FEC) code and LACO-OFDM framework, which invokes carefully harmonised FEC codes for correcting channel errors as well as for eliminating the ILI. Our main contributions in this paper are:

- We quantify the achievable rate of LACO-OFDM systems relying on different modulation schemes and different number of layers, which is based on both the theoretical mutual information and simulations.
- We conceive a novel FEC coded LACO-OFDM system, which intrinsically amalgamates the classic FEC codes with our LACO-OFDM system. Our results demonstrate that the proposed coded LACO-OFDM system significantly outperforms the benchmark system consisting of a separate FEC and LACO-OFDM scheme in terms of its BER performance as well as the decoding complexity.
- We further analyse the layered BER of the proposed coded system. It is demonstrated that the proposed coded LACO-OFDM system is capable of drastically reducing the ILI. Quantitatively, the coded LACO-OFDM system relying on 4-layer 16QAM LACO-OFDM and turbo coding (8-iteration) completely eliminates the ILI at $E_b/N_0 = 10$ dB, which is 9 dB lower than that of the uncoded system.

The structure of this paper is as follows. In Section II we briefly review the uncoded ACO- and LACO-OFDM schemes. The achievable rate of LACO-OFDM is derived in Section III. This is followed by a novel multi-class coded LACO-OFDM architecture in Section IV. Our numerical simulation results, together with our further discussions on the coding performance are given in Section V. Finally, our conclusions are offered in Section VI.

II. System Model

In this section, we introduce the layered model that is used in our system. We first describe the basic transmitter and receiver units of an ACO-OFDM module.

Based on pioneering work on LACO-OFDM [13], we consider the following indoor VLC downlink communication scenario. In our assumption, a single LED acts as the transmitter that serves one user within the room. It has been shown in our previous work [19], that the LACO-OFDM scheme is capable of drastically reducing the signal's PAPR. Therefore, the LED invokes LACO-OFDM for transmission in our system. We assume furthermore that the LED operates within its linear range, hence no clipping occurs, with the maximum allowed transmit energy $E_{\mathrm{LED,max}}$ set according to the LED specifications. This constrains the electrical power of the unipolar TD transmitted signal x at any time instance according to:

$$0 \leq |x[t]|^2 \leq E_{\mathrm{LED,max}}, \quad \forall\, t.$$

In the FD, we normalise the average transmission power of each symbol $X[k]$ to 1, regardless of the number of layers and of the choice of FEC codes, for the sake of a fair comparison, i.e.

$$\frac{1}{K}\sum_{k=0}^{K-1} |X[k]|^2 = 1,$$

where K stands for the total number of symbols transmitted. An additive white Gaussian noise (AWGN) channel is considered in this paper, which is an appropriate assumption for LOS VLC scenarios and has been commonly adopted for IM/DD performance analysis [10], [23], [24]. The optical channel can be modelled in the TD as

$$r = x + n,$$

where r is the received signal. We have not considered the pathloss or fading in this paper, which is a common practice [8]. The TD noise n is expected to be real-valued, and it is defined as

$$n \sim \mathcal{N}\left(0, \frac{\sigma_n^2}{2}\right),$$

where $\frac{\sigma_n^2}{2}$ is the single-sided noise power. Please note that a factor of $\frac{1}{2}$ is incorporated, because only half of the power is associated with the positive frequencies of the noise power spectrum.

A. ACO-OFDM

Figure 1 shows the general schematic of the ACO-OFDM transmitter, relying on M_1-ary QAM. The subscript "1" indicates that this signal constitute the *first* layer of the LACO-OFDM scheme discussed in Sec. II-B. The input bit stream b_1 of length B_1 is mapped onto the complex FD symbols S_1 based on a given M_1-ary quadrature amplitude modulation (M_1QAM) constellation. This provides a total of $B_1/\log_2 M_1$ complex symbols, which, together with their $B_1/\log_2 M_1$ conjugate counterparts and with the additional $2B_1/\log_2 M_1$ null placeholder symbols, are then mapped onto $\mathsf{N}_1 = 4B_1/\log_2 M_1$ subcarriers $\tilde{S}_1$ as follows:

$$\tilde{S}_1[u] = \begin{cases} S_1[k], & u = 2k+1, \\ S_1^*[k], & u = \mathsf{N}_1 - (2k+1), \\ 0, & \text{otherwise}, \end{cases} \tag{1}$$

where * denotes the conjugate of a complex number. Since the FD symbols $\tilde{S}_1$ obey Hermitian symmetry, the TD signal s_1 obtained after inverse fast Fourier transform (IFFT) becomes

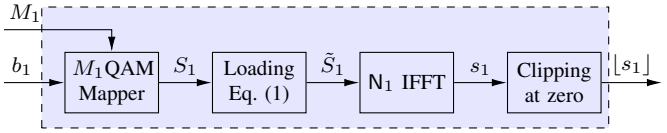

Fig. 1. An ACO-OFDM transmitter block (ACO TX).

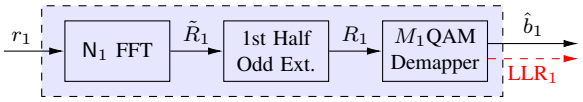

Fig. 2. An ACO-OFDM receiver block (ACO RX).

real-valued and anti-symmetric, i.e. we have $-s_1[k] = s_1[\mathsf{N}_1 - k]$. Therefore, all negative samples of s_1 can be dropped without losing information. The resultant non-negative electric signal $\lfloor s_1 \rfloor$ is converted into optical signal and emitted through an LED.

Figure 2 shows the schematic of the ACO-OFDM receiver. The received signal r_1 is first passed through the FFT to obtain the corresponding FD signal $\tilde{R}_1$. Since the negative clipping distortion only falls on the even-indexed blank subcarriers ($u = 2k$), the desired information can be extracted from the first half odd-indexed subcarriers. The resultant extracted symbols R_1 are then demapped onto the estimated bit stream $\hat{b}_1$. Meanwhile, the demapper may also produce the likelihood ratios (LLRs) of each bit, when operating in a soft output mode.

B. LACO-OFDM

The LACO-OFDM framework utilises the blank even-indexed subcarriers ($u = 2k$) of the classic ACO-OFDM frame for transmitting additional layers of ACO-OFDM symbols, since clipping distortion only exists at the even indices, which can be removed at the receiver. Explicitly, the classic ACO-OFDM relying on N_1-point IFFT/FFT constitutes the first layer ($l = 1$). The $\mathsf{N}_2 = \mathsf{N}_1/2$ blank subcarriers of the first layer are then filled by the second layer ($l = 2$) ACO-OFDM symbol, relying on N_2-point IFFT/FFT. Similarly, additional ACO-OFDM layers can be added, so that the lth layer occupies $\mathsf{N}_l = \mathsf{N}_1/2^{l-1}$ blank subcarriers. A stylised FD view of a 3-layer LACO-OFDM signal is provided in Fig. 3 to demonstrate the subcarrier assignment of the different layers' symbols and their clipping distortions. It is possible to incorporate a maximum of $(\log_2 \mathsf{N}_1 - 1)$ layers in the LACO-OFDM system. However, typically 4 and 5 layers are sufficient to strike an attractive trade-off between the throughput and energy consumption [13], [25].

Figure 4 shows the block diagram of a LACO-OFDM transmitter consisting of L ACO-OFDM blocks as its basic units. The serial input bit stream is firstly split into L parallel streams, corresponding to the L layers, each of which is independently fed to an ACO-OFDM TX unit. It is pertinent to mention that several factors, such as the throughput demand and quality of service (QoS) requirement, dictate both the number of bits B_l (length of b_l) assigned to each layer and the modulation order (M_l) of each layer. However, the

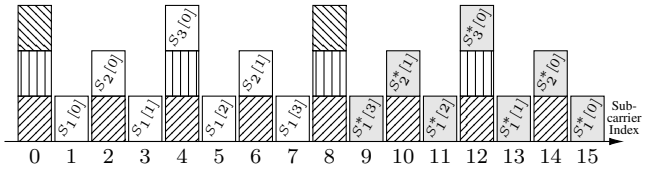

Fig. 3. Frequency domain view of a 3-layer LACO-OFDM signal with 16-point FFT [19]. The purely light shaded bricks with '*' symbols are the Hermitian symmetry conjugates, while the North East hatching, vertical hatching and North West hatching represent distortion generated by Layer 1, 2 and 3, respectively.

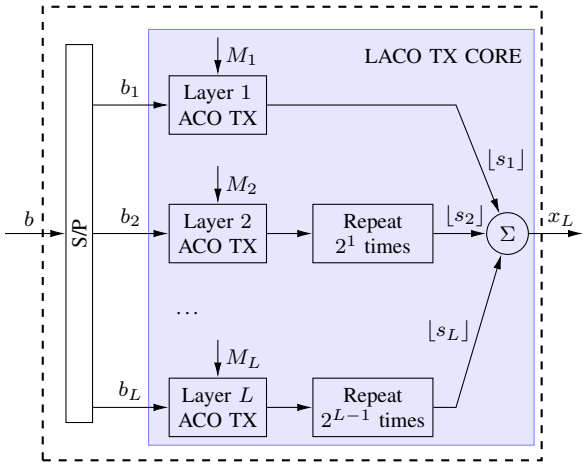

Fig. 4. A LACO-OFDM transmitter system, where ACO TX is a block of Fig. 1.

combination of B_l and M_l must ensure that the lth layer outputs exactly $\mathsf{N}_1/2^{l+1}$ symbols. This in turn implies that the TD signal must repeat itself several times for $l > 1$ for the sake of aligning the TD signals of all the L layers. Finally, the resultant LACO-OFDM signal x_L is now ready for electric/optical conversion.

Recall from Fig. 3 that the first layer is free from ILI, while all the subsequent layers are contaminated by the ILI of the previous layers, *i.e.*, the lth layer is contaminated by the ILI of layers 1 to $(l-1)$. Therefore, the received LACO-OFDM signal is detected in a layer-by-layer manner, invoking SIC for removing the ILI of the previous layers. Explicitly, Fig. 5 shows the block diagram of a LACO-OFDM receiver. The received signal $r_L^{(0)}$ is firstly fed to the 'layer 1 ACO RX', since layer 1 is not contaminated by any ILI. The detected bits $\hat{b}_1$ are then fed to the 'layer 1 ACO TX' for the sake of locally regenerating the clipped signal $\lfloor s_1 \rfloor$ at the receiver as $\lfloor \hat{s}_1 \rfloor$. Next, $\lfloor \hat{s}_1 \rfloor$ is subtracted from the received signal $r_L^{(0)}$, hence resulting in the signal $\hat{r}_L^{(1)}$, which is not contaminated by the ILI of layer 1, provided that the layer bits have been perfectly detected, i.e. we have $\hat{b}_1 = b_1$. This SIC process is repeated for all the subsequent layers, so that the signal $\hat{r}_L^{(L-1)}$ fed to the 'ACO RX' unit of the Lth layer becomes free from the ILI of all the previous layers. Unfortunately, the SIC is not perfect, because any residual errors in the detected bits $\hat{b}_l$ corrupt the regenerated signal $\lfloor \hat{s}_l \rfloor$. Consequently, the ILI is not completely eliminated and the residual ILI of the

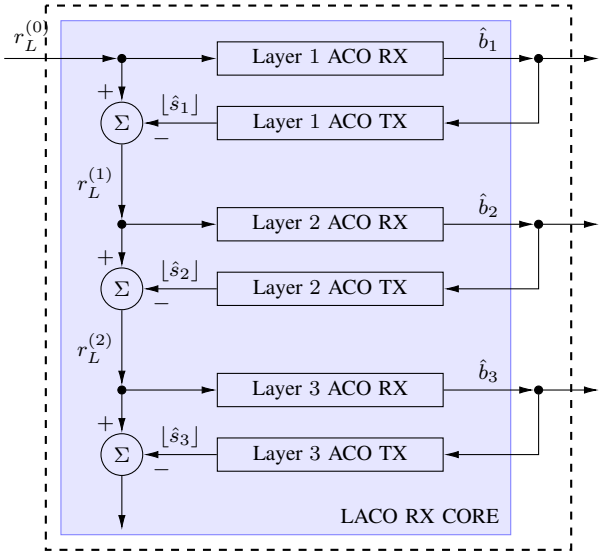

Fig. 5. A LACO-OFDM receiver system, where ACO TX and ACO RX represent the blocks seen in Figs. 1 and 2, respectively.

successive layers accumulates, as we move to higher layers. This in turn implies that the higher layers exhibit a higher BER than the lower ones.

We denote the BER of layer l as $\mathbb{P}_{b,l}$. Under the reasonable assumption that a maximum of one bit error shall occur in each Gray-coded QAM constellation symbol at a sufficiently high SNR, the symbol error rate (SER) of the same layer would be

$$\mathbb{P}_{s,l} = \frac{\text{error symbols}}{\text{total symbols}} = \frac{\mathbb{P}_{b,l} \cdot N_l}{N_l / \log_2 M_l} = \mathbb{P}_{b,l} \log_2 M_l, \quad (2)$$

where the total number of bits N_l within the lth layer is used for intermediate conversion. Meanwhile, for each of the symbol errors, its influence on the locally generated clipped signal $\lfloor \hat{s}_l \rfloor$ is quantified by the square of the Euclidean distance between the correct and corrupted symbol, which equals to the square of the minimum symbol distance in the QAM constellation, given by [14, p. 177]

$$\mathsf{d}_{\min}^{M_l\text{QAM}} = \sqrt{\frac{6}{M_l - 1}}. \quad (3)$$

Therefore, the ILI $\mathcal{G}_l$ generated by layer l can be calculated based on the number of symbol errors and their averaged influence on each of the subcarriers after IFFT, given as [19]

$$\mathcal{G}_l = \mathbb{P}_{s,l} \cdot \left(\mathsf{d}_{\min}^{M_l\text{QAM}}\right)^2 = \frac{6\mathbb{P}_{b,l} \log_2 M_l}{M_l - 1}. \quad (4)$$

While the performance of the first layer is influenced only by the channel AWGN, all higher layers are additionally subjected to the ILI from all previous layers. *e.g.* Layer 3 is influenced by $\mathcal{G}_1$ and $\mathcal{G}_2$, as well as the channel AWGN. Therefore, we define $\Gamma_{s,l}$ as the electric signal-to-noise-and-interference ratio of the lth layer as

$$\Gamma_{s,l} = \frac{\gamma_b N_0 \sum_{l'=1}^{L} (2^{-l'-1} \log_2 M_{l'})}{N_0 + \sum_{i=1}^{l-1} \mathcal{G}_i}, \quad (5)$$

where γ_b is the channel's overall energy-per-bit-to-noise-power-spectral-density ratio and N_0 is the noise power spectral density. Hence, the $\mathbb{P}_{b,l}$ of the LACO-OFDM system can be computed by modifying the standard QAM BER formula from [14] as follows

$$\mathbb{P}_{b,l} \approx \frac{4(\sqrt{M_l} - 1)}{\sqrt{M_l} \cdot \log_2 \sqrt{M_l}} \cdot Q\left(\sqrt{\frac{3\Gamma_{s,l} \log_2 M_l}{M_l - 1}}\right). \quad (6)$$

III. Achievable Rate Analysis

Li *et al.* [26] derived a tight bound on the capacity of the general IM/DD channel based on the probability density function (PDF) of both the optical signal and the noise. They also provided the channel capacity of ACO-OFDM, which is essentially a quarter of Shannon's capacity [27]. As a further advance, the upper bound of the multicarrier optical IM/DD capacity was quantified by You and Khan [28] with the help of trigonometric moment sequences, while Hranilovic and Kschischang [29] studied both the upper and lower bound of an AWGN optical IM/DD channel. A tighter capacity upper bound is derived by Chaaban *et al.* [30]. In [31], the capacity for parallel optical channels were studied. The capacity bounds for bandlimited optical intensity channels were given in [32]. More recently, Zhou *et al.* derived the continuous-input continuous-output memoryless channel (CCMC) capacity, also known as the unrestricted bound, of LACO-OFDM [33]. Inspired by these advances, in this section we quantify the achievable rate [34] of a LACO-OFDM system relying on different number of layers and different modulation schemes, which has not been studied in the open literature. Naturally, the achievable rate of a LACO-OFDM system increases, as more layers are incorporated and higher-order modulation schemes are used. The achievable rate derived in this section will be subsequently used in Sec. V for benchmarking the performance of the proposed coded LACO-OFDM system.

A. achievable rate for ACO-OFDM

Let us first analyse a simple single-layer LACO-OFDM system, which is basically ACO-OFDM. We once again used the subscript "1" for all the ACO-OFDM symbols, since this ACO-OFDM system constitutes the first layer of LACO-OFDM. If an FD symbol $S_1[k]$ is transmitted from TX of Fig. 1, the FD symbol received at the RX side can be expressed as

$$R_1[k] = S_1[k] + N, \quad (7)$$

where N is the halved power-effective AWGN represented in the FD. Let $d_{1,k,m}$ be the Euclidean distance between the received symbol $R_1[k]$ and the mth symbol $\mathcal{S}^{(m)}$ of the M_1QAM constellation set $\mathcal{S}$ ($m = 0, 1, \ldots, M_1 - 1$), which is given by:

$$d_{1,k,m} = \left\| R_1[k] - \mathcal{S}^{(m)} \right\| = \left\| S_1[k] + N - \mathcal{S}^{(m)} \right\|, \quad (8)$$

where $\|\cdot\|$ is the l_2-norm operator. Then the soft channel information $\mathbb{P}\left(R_1[k] \mid S_1[k] = \mathcal{S}^{(m)}\right)$, which denotes the probability of receiving the symbol $R_1[k]$ at the kth instant when $S_1[k] = \mathcal{S}^{(m)}$ is transmitted, is computed by the demapper

using the distance $d_{1,k,m}$ and the Gaussian-distributed noise N as [34]

$$\mathbb{P}\left(R_1[k] \mid S_1[k] = \mathcal{S}^{(m)}\right) = \frac{\exp\left[-\dfrac{d^2 1, k, m}{\sigma_n^2/2}\right]}{\pi \cdot \sigma_n^2/2}. \quad (9)$$

Here, $\sigma_n^2/2$ is the power of the effective AWGN N of (7), which may be expressed as

$$N \sim \mathcal{CN}\left(0, \frac{\sigma_n^2}{2}\right). \quad (10)$$

It is pertinent to mention that if the channel SNR is $\frac{E_s}{N_0}$ for unit symbol energy, then the effective noise power may be estimated by:

$$\frac{E_s}{N_0} = \gamma_b \cdot \left(\frac{1}{4}\log_2 M_1\right) = \frac{1}{\sigma_n^2/2}, \quad (11)$$

which yields

$$\frac{\sigma_n^2}{2} = \frac{1}{\gamma_b \cdot \frac{1}{4}\log_2 M_1} \quad (12)$$

for ACO-OFDM.

Using Bayes's Theorem, the *a posteriori* probability of the transmitted symbol $S_1[k] = \mathcal{S}^{(m)}$ given a received symbol $R_1[k]$ becomes:

$$\begin{aligned}&\mathbb{P}\left(S_1[k] = \mathcal{S}^{(m)} \mid R_1[k]\right)\\ &= \frac{\mathbb{P}\left(R_1[k] \mid S_1[k] = \mathcal{S}^{(m)}\right) \cdot \mathbb{P}\left(S_1[k] = \mathcal{S}^{(m)}\right)}{\mathbb{P}\left(R_1[k]\right)}.\end{aligned} \quad (13)$$

Since the transmitted symbols are uniformly distributed over the same constellation pattern, the *a priori* probability for any of the M_1 transmitted symbols is given by

$$\mathbb{P}\left(S_1[k] = \mathcal{S}^{(m)}\right) = \frac{1}{M_1} \quad \forall m. \quad (14)$$

Furthermore, the probability of received symbols $R_1[k]$ may be computed using:

$$\begin{aligned}\mathbb{P}\left(R_1[k]\right) = \sum_{m=1}^{M_1} \Big[&\mathbb{P}\left(R_1[k] \mid S_1[k] = \mathcal{S}^{(m)}\right) \times\\ &\mathbb{P}\left(S_1[k] = \mathcal{S}^{(m)}\right)\Big].\end{aligned} \quad (15)$$

Substituting (14) and (15) into (13) yields:

$$\begin{aligned}&\mathbb{P}\left(S_1[k] = \mathcal{S}^{(m)} \mid R_1[k]\right)\\ &= \frac{\mathbb{P}\left(R_1[k] \mid S_1[k] = \mathcal{S}^{(m)}\right)}{\sum_{m=1}^{M_1} \mathbb{P}\left(R_1[k] \mid S_1[k] = \mathcal{S}^{(m)}\right)}.\end{aligned} \quad (16)$$

Hence, (16) implies that $\mathbb{P}\left(S_1[k] = \mathcal{S}^{(m)} \mid R_1[k]\right)$ is equivalent to the *normalised counterpart* of $\mathbb{P}\left(R_1[k] \mid S_1[k] = \mathcal{S}^{(m)}\right)$, when the transmitted symbols S_1 are equiprobable. Consequently, $H(\mathsf{R}_1|\mathsf{S}_1)$ relies on the un-normalised probabilities $\mathbb{P}\left(R_1[k] \mid S_1[k] = \mathcal{S}^{(m)}\right)$, while $H(\mathsf{S}_1|\mathsf{R}_1)$ relies on the normalised probabilities $\frac{\mathbb{P}\left(R_1[k]|S_1[k]=\mathcal{S}^{(m)}\right)}{\sum_{m=1}^{M_1}\mathbb{P}\left(R_1[k]|S_1[k]=\mathcal{S}^{(m)}\right)}$.

According to Shannon's theorem [27], the capacity C of a channel is equivalent to the maximum information conveyed, which equals to the entropy of the source minus the average information lost. The achievable rate $\mathbb{R}$ is then upper-bounded by the capacity for the sake of a error-free transmission, which is expressed as

$$\mathbb{R} \leq C = \max I(\mathsf{S}, \mathsf{R}) = \max\left[H(\mathsf{S}) - H(\mathsf{S}|\mathsf{R})\right], \quad (17)$$

where $I(\cdot\ ,\ \cdot)$ is the mutual information function and $H(\cdot)$ is the information entropy function, while S stands for the source/Tx and R the sink/Rx. Many thanks for highlighting this. As discussed in response to your Comment 11, we have considered equiprobable source symbols, which maximize the transmission rate for the noiseless scenario. Hence, we have modified our statement as follows: Since we have considered equiprobable source symbols, we have [35], [36]

$$H(\mathsf{S}_1)^{\mathrm{ACO}} = \frac{\mathsf{N}_1}{\mathsf{N}}\log_2 M_1 = \frac{1}{4}\log_2 M_1, \quad (18)$$

while $H(\mathsf{S}_1|\mathsf{R}_1)^{\mathrm{ACO}}$ is given in (19), where $\mathbb{P}\left(R_1[k] \mid S_1[k] = \mathcal{S}^{(m)}\right)$ is computed using (9). The term of $\frac{\mathsf{N}_1}{\mathsf{N}} = \frac{1}{4}$ incorporated in both (18) and (19) indicates the four-fold spectral efficiency reduction of ACO-OFDM, where N is the total number of subcarriers available, and N_1 is the number of symbols transmitted using the ACO-OFDM scheme [8], [26]. Explicitly, the expectation operator $\mathbb{E}\{\cdot\}$ of (19) computes the average of all TD symbols across all occupied subcarriers. Therefore, a factor of $\frac{\mathsf{N}_1}{\mathsf{N}}$ has to be incorporated to get the average entropy of a LACO-OFDM frame.

Finally, the achievable rate of an ACO-OFDM system can be expressed as

$$\mathbb{R}^{\mathrm{ACO}}_{M_1\mathrm{QAM}} = \frac{\log_2 M_1}{4} - H(\mathsf{S}_1|\mathsf{R}_1)^{\mathrm{ACO}} \text{ bits/symbol}. \quad (20)$$

B. achievable rate for LACO-OFDM

Next, we extend the aforementioned achievable rate analysis to the more complex LACO-OFDM system, which also relies on the classic information theoretic capacity and achievable rate (17).

For an L-layer LACO-OFDM scheme, the overall conveyed information quantified by the channel capacity can be expressed as

$$C = I(\mathsf{S}_1, \mathsf{S}_2, \ldots, \mathsf{S}_L\ ;\ \mathsf{R}_1, \mathsf{R}_2, \ldots, \mathsf{R}_L), \quad (21)$$

where the first half represents the source symbols of each layer, while the second half denotes their corresponding sink symbols. Recall that each layer of LACO-OFDM is an ACO-OFDM signal and the transmitted symbols of each layer are independent, while the received symbols are correlated due to the presence of ILI. Therefore, (21) can be rearranged as

$$\begin{aligned}C = &I(\mathsf{S}_1\ ;\ \mathsf{R}_1, \mathsf{R}_2, \ldots, \mathsf{R}_L) + I(\mathsf{S}_2\ ;\ \mathsf{R}_1, \mathsf{R}_2, \ldots, \mathsf{R}_L)\\ &+ \cdots + I(\mathsf{S}_l\ ;\ \mathsf{R}_1, \mathsf{R}_2, \ldots, \mathsf{R}_L) + \cdots\\ &+ I(\mathsf{S}_L\ ;\ \mathsf{R}_1, \mathsf{R}_2, \ldots, \mathsf{R}_L).\end{aligned} \quad (22)$$

For the sake of simplifying this cascaded ILI in the capacity calculation, we exploit the widely used chain rule [37]. Consequently, each of the terms in (22) can be rewritten as

$$\begin{aligned}&I(\mathsf{S}_l\ ;\ \mathsf{R}_1, \mathsf{R}_2, \ldots, \mathsf{R}_l,\ \ \mathsf{R}_{l+1}, \ldots, \mathsf{R}_L)\\ &= I(\mathsf{S}_l; \mathsf{R}_1, \ldots, \mathsf{R}_l) + I(\mathsf{S}_l; \mathsf{R}_{l+1}, \ldots, \mathsf{R}_L|\mathsf{R}_1, \ldots, \mathsf{R}_l).\end{aligned} \quad (23)$$

$$
\begin{aligned}
H(\mathsf{S}_1|\mathsf{R}_1)^{\mathrm{ACO}} &= \frac{\mathsf{N}_1}{\mathsf{N}}\,\mathbb{E}\left\{-\sum_{m=1}^{M_1}\left[\mathbb{P}\left(S_1[k]=\mathcal{S}^{(m)},\ R_1[k]\right)\cdot\log_2\mathbb{P}\left(S_1[k]=\mathcal{S}^{(m)}\mid R_1[k]\right)\right]\right\}\\
&= \frac{\mathsf{N}_1}{\mathsf{N}}\,\mathbb{E}\left\{-\sum_{m=1}^{M_1}\left[\mathbb{P}\left(R_1[k]\mid S_1[k]=\mathcal{S}^{(m)}\right)\cdot\mathbb{P}\left(S_1[k]=\mathcal{S}^{(m)}\right)\cdot\log_2\mathbb{P}\left(S_1[k]=\mathcal{S}^{(m)}\mid R_1[k]\right)\right]\right\} \qquad (19)\\
&= \frac{1}{4}\,\mathbb{E}\left\{-\frac{1}{M_1}\sum_{m=1}^{M_1}\left[\mathbb{P}\left(R_1[k]\mid S_1[k]=\mathcal{S}^{(m)}\right)\cdot\log_2\frac{\mathbb{P}\left(R_1[k]|S_1[k]=\mathcal{S}^{(m)}\right)}{\sum_{m'=1}^{M_1}\mathbb{P}\left(R_1[k]|S_1[k]=\mathcal{S}^{(m')}\right)}\right]\right\},
\end{aligned}
$$

Recall that each layer is only affected by the ILI of lower layers. Consequently, the symbols R_l received in the lth layer are independent of the symbols $\{R_{l+1}, R_{l+2}, \ldots, R_L\}$ received in the upper layers. Hence, the second term in (23) is always zero, while the first term can be further expanded as

$$I(\mathsf{S}_l\ ;\ \mathsf{R}_1,\ldots,\mathsf{R}_l) = H(\mathsf{S}_l) - H(\mathsf{S}_l\mid\mathsf{R}_1,\ldots,\mathsf{R}_l), \qquad (24)$$

which is the source entropy of the lth layer, minus the loss of information caused by all the $(1\sim l)$th layers.

As it will be demonstrated in Sec. V-B, the ILI can be substantially reduced by appropriately incorporating FEC codes. Hence, under the assumption of perfect error correction (or equivalently, perfect detection), the ILI can be completely eliminated. Consequently, it is reasonable to assume that we have:

$$H(\mathsf{S}_l\mid\mathsf{R}_1,\ldots,\mathsf{R}_l)\approx H(\mathsf{S}_l\mid\mathsf{R}_l),\quad \forall 1\le l\le L, \qquad (25)$$

where $H(\mathsf{S}_l\mid\mathsf{R}_l)$ related to the lth layer can be computed using (19). This in turn implies that the overall conveyed information can be estimated by adding together the information conveyed by each independent ACO-OFDM layer.

Hence, the achievable rate of an L-layer LACO-OFDM system can be expressed in bits/symbol as follows:

$$\mathbb{R}^{L\mathrm{ACO}}_{\{M_l\}\mathrm{QAM}} = \sum_{l=1}^{L} 2^{-l-1}\left[\log_2 M_l - H(\mathsf{S}_l\mid\mathsf{R}_l)\right], \qquad (26)$$

where the factor 2^{-l-1} denotes the spectrum efficiency of the lth layer as in [19]. If all layers invoke the same modulation scheme, i.e. we have $M_l = M$, $\forall\ l$, then (26) can be further simplified as follows:

$$\mathbb{R}^{L\mathrm{ACO}}_{M\mathrm{QAM}} = \frac{\left(1-2^{-L}\right)}{2}\left[\log_2 M - H(\mathsf{S}_1\mid\mathsf{R}_1)\right]\ \text{bits/symbol}, \qquad (27)$$

since $H(\mathsf{S}_l\mid\mathsf{R}_l)\equiv H(\mathsf{S}_1\mid\mathsf{R}_1)$ and $\sum_{l=1}^{L}2^{-l-1} = \frac{1}{4}+\frac{1}{8}+\cdots+\frac{1}{2^{L+1}} = (1-2^{-L})/2$.

It is also worth mentioning that when calculating $H(\mathsf{S}_1\mid\mathsf{R}_1)$ for LACO-OFDM, the noise power should be higher for a given value of $\frac{E_s}{N_0}$, because the total symbol energy increases as more layers are superimposed and more idle subcarriers are filled up. More specifically, if equal symbol energy is assigned to every subcarrier, as in [13], [19], then the total unnormalised LACO-OFDM symbol power is equivalent to [19]

$$E_s = \frac{2}{\pi}\left[\frac{\left(1-2^{-L/2}\right)^2}{3-2\sqrt{2}} + (\pi-1)\left(1-\frac{1}{2^L}\right)\right]. \qquad (28)$$

Consequently, (11) should be modified as

$$\frac{E_s}{N_0} = \gamma_b\cdot\sum_{l=1}^{L}\left(\frac{1}{2^{l+1}}\cdot\log_2 M_l\right) = \frac{E_s}{\sigma_n^2/2}, \qquad (29)$$

which in turn modifies (12) into

$$\frac{\sigma_n^2}{2} = \frac{\frac{2}{\pi}\left[\frac{\left(1-2^{-L/2}\right)^2}{3-2\sqrt{2}} + (\pi-1)\left(1-\frac{1}{2^L}\right)\right]}{\gamma_b\cdot\sum\limits_{l=1}^{L}\left(\frac{1}{2^{l+1}}\cdot\log_2 M_l\right)} \qquad (30)$$

for LACO-OFDM.

C. Numerical Results and Summary

In this subsection, we present our numerical LACO-OFDM achievable rate results. Obtaining analytical results would be a complex task due to the logarithm operation in (19). Hence we invoke Monte-Carlo simulations here.

Figure. 6 shows the IM/DD optical DCMC capacities of different LACO-OFDM systems. More specifically, Fig. 6a portrays the achievable rate of a 3-layer LACO-OFDM, while Fig. 6b that of a 4-layer system. Three QAM constellation sizes, namely 4QAM, 16QAM and 64QAM, are used for comparison. As illustrated in Fig. 6, LACO-OFDM having more layers offers a higher achievable rate, since all three curves seen in Fig. 6b converge to slightly higher values than their counterparts in Fig. 6a.

In this section, we derived the achievable rate of the LACO-OFDM system. We started by deriving the *a posteriori* probability and the conditional entropy of the transmitted symbols, which helps in calculating the average amount of information conveyed through the channel, known as the DCMC capacity and upper-bounds the achievable rate. Next we proved that the achievable rate of a LACO-OFDM system can be approximated as the sum of the ACO-OFDM layers' DCMC capacity, in the absence of of ILI. The choice of modulation schemes on each layer is further considered, which influences this layer's contribution to the total achievable rate. The achievable rate versus SNR curves are then illustrated, which will help us determine the achievable rate limit for a given coding rate, as it will be detailed in Sec. V.

IV. Layered ACO-OFDM with Channel Coding

A naive coded LACO-OFDM system can be formulated by simply concatenating an FEC code to a LACO-OFDM

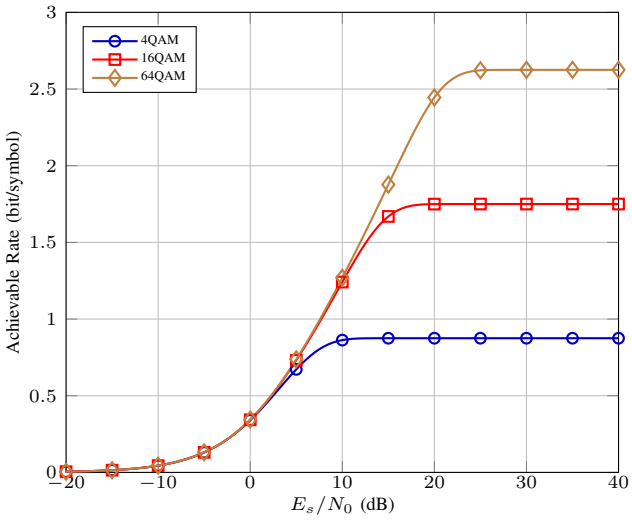

(a) 3-layer LACO-OFDM

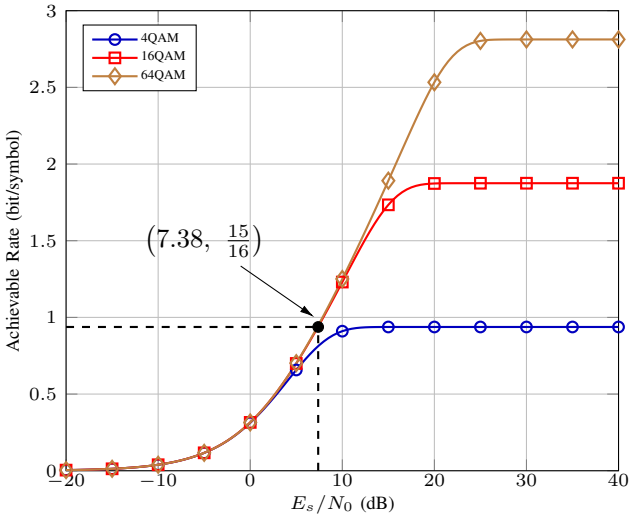

(b) 4-layer LACO-OFDM

Fig. 6. IM/DD optical achievable rate of LACO-OFDM system using different number of layers and different QAM constellation sizes.

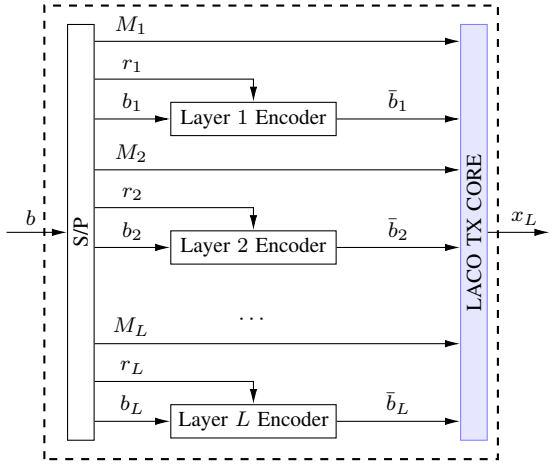

Fig. 7. A LACO-OFDM transmitter integrated with FEC encoders. The 'LACO TX CORE' block is given in Fig. 4.

module, referred to as a single-class structure. Explicitly, the bit stream b of Fig. 4 is FEC-encoded before being fed to the S/P module of LACO-OFDM. Similarly, the detected bit stream $\hat{b}$ of Fig. 5 is decoded by FEC decoders after all of its segments $\left\{\hat{b}_l\right\}_{l=1}^{L}$ have been detected. However, this structure has several impediments that limit its overall performance.

1) The original TX of Fig. 4 has a parallel structure. The signal processing of all layers can be carried out simultaneously, before their respective clipped signals are superimposed onto each other. However, in case of the conventional single-class coded LACO-OFDM system, the encoder operates serially. Hence, the higher layers have to wait for their bits to be encoded. This introduces delay at the TX. It is also worth noting that the delay increases upon increasing the frame length.
2) The conventional coded LACO-OFDM system fails to exploit the full potential of FEC codes. The FEC codes are capable of alleviating the impact of ILI, if invoked in a carefully matched layered manner. As it will be detailed later in this section, ILI in the conventional system is the same as that in the uncoded system.
3) One of the benefits of a LACO-OFDM system is its flexibility [19]. Specifically, the number of layers, the modulation scheme as well as the power allocation invoked for each layer can be adjusted to achieve a desired QoS or throughput requirement. However, since all bits are encoded jointly in a single-class coded system, the same coding rate, and more importantly the same code, must be used for all input bits; hence, the system loses flexibility. This can be particularly disadvantageous in scenarios, where one would like to use stronger codes for particular layers to provide a higher level of protection.

Against this background, we present our new multi-class coded LACO-OFDM system, where the encoding and decoding components are integrated within the original layered structure. In this way, the system avoids the aforementioned problems, since each layer has its own encoding and decoding units.

A. Encoder Design

Figure 7 shows the schematic of the proposed multi-class LACO-OFDM transmitter, which intrinsically integrates layer-specific FEC encoders within the layered structure of the LACO-OFDM system. Each layer of the LACO-OFDM system of Fig. 7 has its own choice of constellation size M_l, coding rate r_l as well as the type of FEC code. First, the S/P block divides the input bit stream b into L blocks, so that the lth layer has B_l uncoded bits, denoted as b_l. Each layer then independently encodes its input bits b_l using an FEC code having a coding rate of r_l. The resultant encoded bits $\bar{b}_l$ and the desired constellation size M_l are then fed to the 'LACO TX CORE' block of Fig. 4 for further processing.

The multi-class FEC encoder of Fig. 7 simultaneously processes each layer. Since each layer only has a portion of the original bit stream b, it takes shorter time to complete the entire encoding process. Moreover, this design allows us to

individually choose the FEC code type and the coding rate for each layer, hence facilitating adaptive LACO-OFDM FEC coding.

B. Decoder Design

Figure 8 shows the schematic of the proposed LACO-OFDM RX, where the FEC decoders are integrated into the multi-class coded structure of LACO-OFDM, similar to the transmitter of Fig. 7. Analogously to the uncoded RX of Fig. 5, the RX of Fig. 8 operates layer-wise, commencing from the first layer, which is not contaminated by ILI. However, the clipped signal $\lfloor s_l \rfloor$ of the lth layer is now regenerated based on the output of the FEC decoder, rather than relying on the hard-output of the QAM demapper. More specifically, the soft QAM demapper of Fig. 8 computes the *a priori* LLRs $L_a\left(\bar{b}_l\right)$ of the encoded bits $\bar{b}_l$ from the bit-based couterparts of the symbol-based likelihood probabilities of (9). The *a priori* LLRs $L_a\left(\bar{b}_l\right)$ are then fed to the FEC decoder of Fig. 8, which is essentially a soft-in-soft-out (SISO) decoder. This SISO decoder yields the *a posteriori* LLRs $L_p\left(b_l\right)$ of the uncoded bits b_l. Finally, hard-decision is applied both to $L_p\left(\bar{b}_l\right)$ and to $L_p\left(b_l\right)$, yielding $\hat{b}_l$ and $\hat{\bar{b}}_l$, respectively. The resultant b_l is then fed to the 'ACO TX' block of Fig. 1 for estimating the ILI imposed on the $(l+1)$st layer. The rest of the process at RX of Fig. 8 is the same as that of the uncoded system. Hence, the proposed RX estimates the ILI based on the output of the FEC decoder. Since the FEC decoder corrects most of the channel errors, the resultant ILI estimations become more accurate. Consequently, the ILI is substantially reduced, provided that the receiver design of Fig. 8 is invoked. Therefore, the FEC encoders of Fig. 8 substantially mitigate the impact of ILI.

V. Simulations and Discussions

In this section, we evaluate the performance of our proposed multi-class coded system. First we benchmark the BER performance against the single-class coded LACO-OFDM system as well as the achievable rate limit. Then we will analyse the detailed influence of FEC codes on each LACO-OFDM layer. In all simulations we have used a 4-layer LACO-OFDM scheme communicating through an AWGN channel relying on a total of 2048 subcarriers and 16QAM.

Furthermore, we have used a $\frac{1}{2}$-rate FEC code for each layer. Hence, the overall throughput (or rate) of the resultant coded LACO-OFDM system can be formulated as follows:

$$\begin{aligned}\mathbb{R}^{\text{4LACO}}_{\text{16QAM}}\big|_{r=1/2} &= \frac{1}{2} \times \left(\log_2(16) \times \frac{1}{4} \times \sum_{l=1}^{4} \frac{1}{2^{l-1}} \right) \\ &= \frac{15}{16} \text{ bits/symbol.}\end{aligned} \tag{31}$$

Based on Shannon's information theorem [27], the achievable rate under such throughput would be $\frac{15}{16}$ bits/symbol, which corresponds to a limit SNR $E_s/N_0 = 7.38$ dB (or equivalently $\gamma_b = 7.66$ dB) according to Fig. 6b.

TABLE I
Channel Coding Schemes Used for Fig. 9

Scheme	Structure	Code	Parameter	States
1	Single-Class	N/A	N/A	N/A
2		Convolutional	$M = 2$	4
3		Turbo	$M = 3$, $I = 8$	128
4	Multi-Class	Convolutional	$M = 2$	4
5			$M = 5$	32
6			$M = 6$	64
7			$M = 7$	128
8		Turbo	$M = 3$, $I = 2$	32
9			$M = 3$, $I = 4$	64
10			$M = 3$, $I = 8$	128

A. Performance Evaluation of Different FEC Codes

Figure 9 shows the BER performance recorded for different coding scenarios listed in Table I. Specifically, we have invoked both convolutional codes having a memory of M and turbo codes relying on I decoding iterations. The performance is benchmarked against the corresponding single-class scenarios as well as the achievable rate limit.

We may observe in Fig. 9 that the multi-class scheme 4 and scheme 8 significantly outperform their single-class counterparts of scheme 2 and scheme 3, respectively. Quantitatively, the layered turbo coded system scheme 8 operates within 1.1 dB of the achievable rate at a BER of 10^{-3}, while that of the single-class turbo coded system is 4.7 dB away from the achievable rate. Hence, our layered design offers a 3.6 dB gain at the same encoding and decoding complexity. We may also observe in Fig. 9 that even the less sophisticated layered convolutional coded scheme 4 of Table I outperforms the single-class turbo coded scheme 3, which has a significantly higher decoding complexity.

More explicitly, the decoding complexity as well as time delay of trellis codes is proportional to the number of trellis states invoked during the decoding process [14]. A memory-2 convolutional code invokes only $2^2 = 4$ trellis states. By contrast, a turbo code relying on two parallel concatenated memory-3 convolutional codes invokes $(2^3 \times 2) = 16$ states in each iteration; hence invoking a total of $(16 \times 8) = 128$ states in 8 iterations. This implies that the layered convolutional-coded system imposes 32 times lower decoding decoding complexity than the single-class turbo-coded system in addition to providing a better BER performance. In Fig. 10 we plot the distance to the achievable rate limit versus coding complexity for a 4-layer LACO-OFDM system utilising the proposed multi-class coding architecture. The coding complexities are quantified by the number of states used, and are also summarised in Table I. As shown in Fig. 10, a closer match to the achievable rate limit can be obtained upon increasing the coding complexity by increasing the memory of the convolutional codes and the number of turbo iterations.

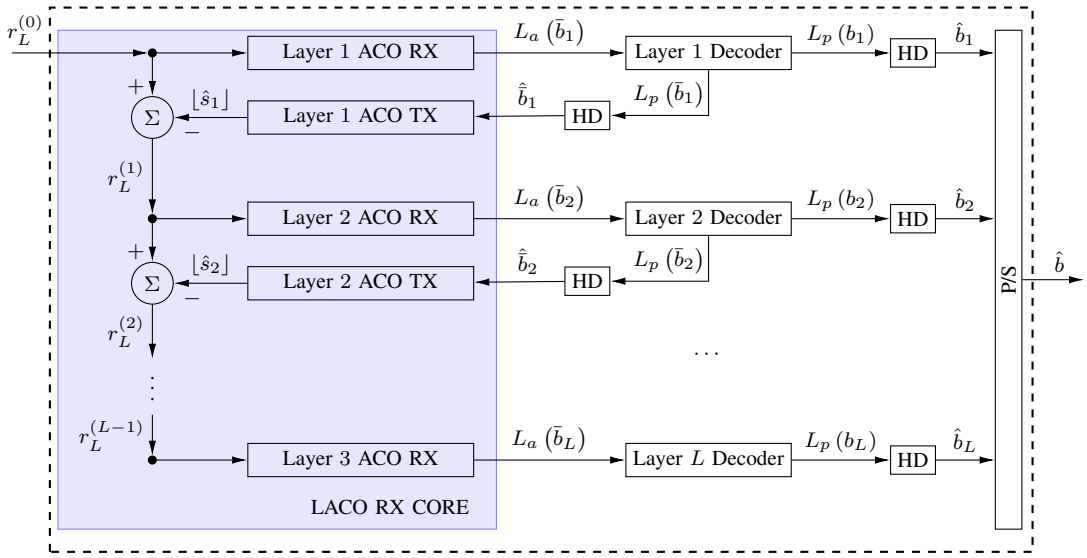

Fig. 8. A LACO-OFDM receiver integrated with FEC decoders. $L_a(\cdot)$ and $L_p(\cdot)$ represent the *a priori* and the *a posteriori* LLR, respectively.

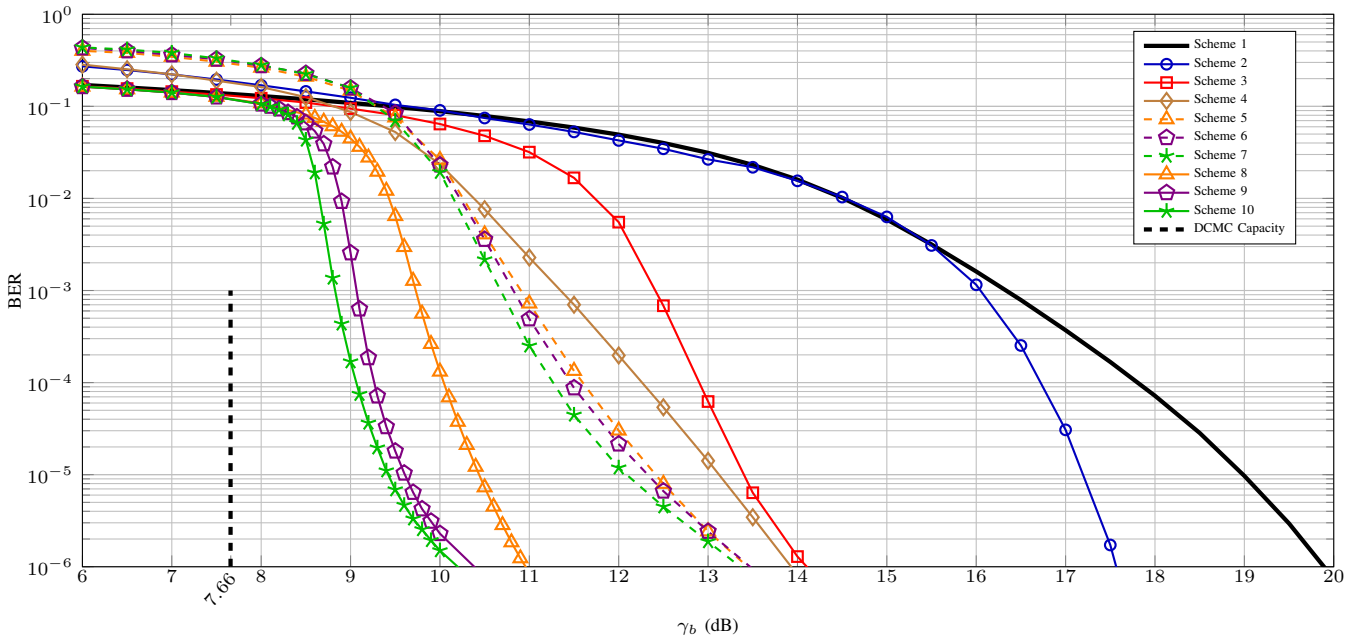

Fig. 9. BER performance of a 4-layer LACO-OFDM system operating 16QAM on all of its layers communicating in AWGN channels. The channel coding schemes of Table I are used.

B. Performance Evaluation for Different LACO-OFDM Layers

Next, we embark on a more detailed analysis of the coding of each LACO-OFDM layer. Turbo coding with a maximum $I = 8$ iterations (scheme 10 of Table I) is considered here owing to its best performance.

Figure 11a records the layer-wise BER performance of the uncoded system, while Fig. 11b depicts the BER performance of the layered turbo coded system. We may observe a dramatic performance improvement for all layers. However, the BER curves of the layers in the turbo-coded scenario do not converge even for very high SNRs. This is because the turbo interleaver length is reduced, as we move up the layers and the performance of the turbo code degrades upon decreasing the interleaver length. More specifically, the first layer has a turbo interleaver length of 2^{11} bits, while that of the fourth layer is only 2^8. Consequently, the turbo code of the first layer performs better than that of the fourth layer, since it is widely recognised that the performance of the turbo code improves upon increasing the interleaver length.

For the sake of demonstrating that the coded system is capable of completely eliminating the ILI, in the investigation of Fig. 12 we use a frame length of 2^8 bits for all layer. Since the first three layers are capable of conveying more bits, their input frames are partitioned into sub-frames of length 2^8, which are encoded (and similarly decoded) separately. The resultant

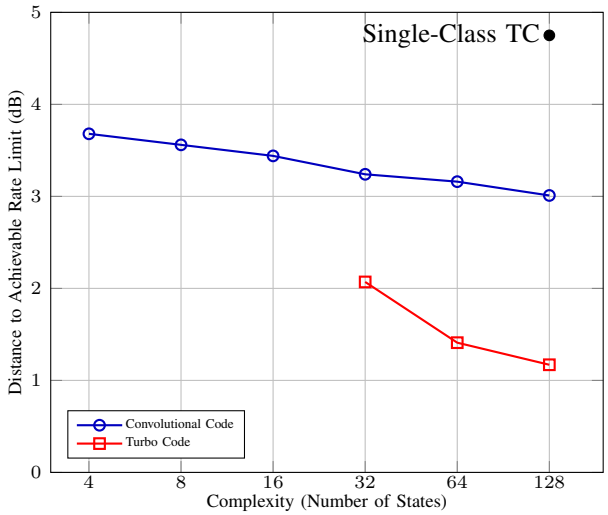

Fig. 10. Distance to the achievable rate limit for multi-class coded 4-layer LACO-OFDM using different coding schemes. Convolutional code with various memory size and turbo code concatenating two memory-3 convolutional code with various iterations are used.

BER performance curves are recorded in Fig. 12. As shown in Fig. 12, all layers now converge around BER $= 10^{-5}$, which echoes the same trend as that in Fig. 11a. This implies that the layered turbo coded system is capable of completely eliminating the ILI around $E_b/N_0 = 10$ dB. By contrast, this was only possible around $E_b/N_0 = 19$ dB in the uncoded regime, as demonstrated in Fig. 11a.

VI. Conclusions

In this paper, a layered channel coding system was proposed for optical IM/DD communications. We first detailed the LACO-OFDM system architecture, and derived the achievable rate with the aid of our mutual information analysis. Next, we discussed the limitations of the single-class system, which was followed by the introduction of our proposed layered LACO-OFDM architecture. Finally, we quantified the benefits of the proposed coded optical communications system by invoking both convolutional and turbo codes. Quantitatively, it was demonstrated that our turbo coded system operated within 1.1 dB of the achievable rate at a BER of 10^{-3}. Furthermore, our convolutional coded system outperformed the single-class turbo coded system despite the 32 times lower decoding complexity of the former. We also demonstrated that the layered coded system is capable of drastically reducing the ILI.

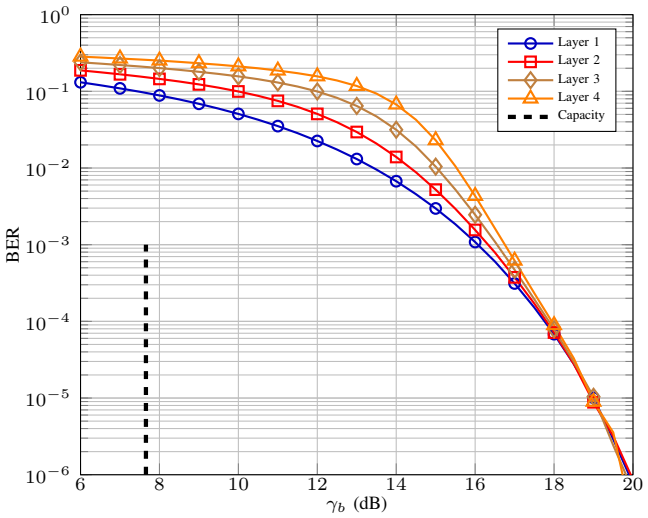

(a) Without FEC [19]

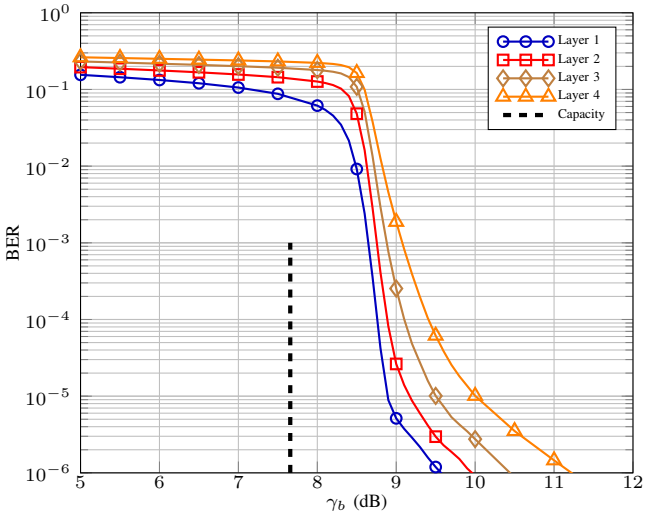

(b) With FEC

Fig. 11. BER performance on each layer of a 4-layer LACO-OFDM system operating 16QAM on all of its layers communicating in AWGN channels. (a) without FEC. (b) with 8-iteration turbo code, and each layer having its maximum achievable interleaver length.

References

[1] L. Hanzo, H. Haas, S. Imre, D. O'Brien, M. Rupp, and L. Gyongyosi, "Wireless myths, realities, and futures: From 3G/4G to optical and quantum wireless," *Proc. IEEE*, vol. 100, pp. 1853–1888, May 2012.

[2] Z. Wang, Q. Wang, W. Huang, and Z. Xu, *Visible light communications: Modulation and signal processing*. Hoboken, New Jersey: Wiley-IEEE Press, 2018.

[3] P. H. Pathak, X. Feng, P. Hu, and M. Mohapatra, "Visible light communication networking and sensing: a survey potential and challenges," *IEEE Commun. Surveys & Tutorials*, vol. 17, pp. 2047–2077, Sep. 2015.

[4] C. Zhu, Y. Huo, J. Jiang, H. Sun, C. Dong, R. Zhang, and L. Hanzo, "Hierarchical colour-shift-keying aided layered video streaming for the visible light downlink," *IEEE Access*, vol. 4, pp. 3127–3152, 2016.

[5] J. M. Kahn and J. R. Barry, "Wireless infrared communications," *Proc. IEEE*, vol. 85, pp. 265–198, Feb. 1997.

[6] L. Hanzo, M. Münster, B. J. Choi, and T. Keller, *OFDM and MC-CDMA for broadband multi-user communications, WLANs and broadcasting*. Chichester: Wiley-IEEE Press, 2003.

[7] G. Zhang, M. De Leenheer, A. Morea, and B. Mukherjee, "A survey on OFDM-based elastic core optical networking," *IEEE Commun. Surveys & Tutorials*, vol. 15, pp. 65–87, Feb. 2013.

[8] J. Armstrong, "OFDM for optical communications," *J. Light. Technol.*, vol. 27, pp. 189–204, Feb. 2009.

[9] J. B. Carruthers and J. M. Kahn, "Multiple-subcarrier modulation for nondirected wireless infrared communication," *IEEE J. Sel. Areas Commun.*, vol. 14, pp. 538–546, Apr. 1996.

[10] J. Armstrong and B. J. C. Schmidt, "Comparison of asymmetrically clipped optical OFDM and DC-biased optical OFDM in AWGN," *IEEE Commun. Lett.*, vol. 12, pp. 343–345, May 2008.

[11] R. Mesleh, H. Elgala, and H. Haas, "On the performance of different OFDM based optical wireless communication systems," *IEEE/OSA J. Opt. Commun. Netw.*, vol. 3, pp. 620–628, Aug. 2011.

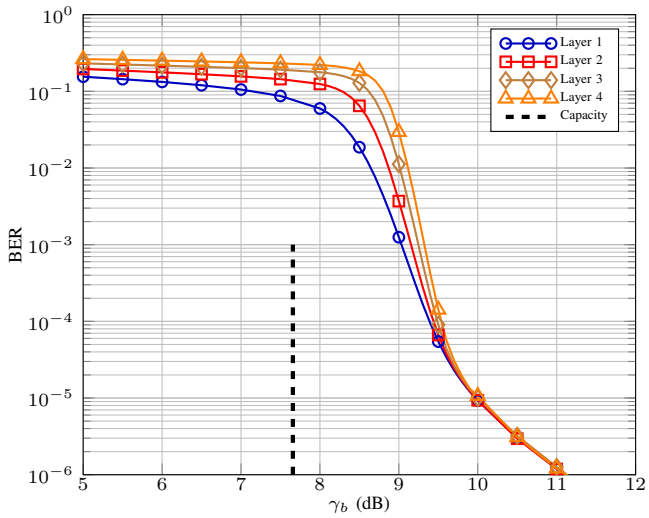

Fig. 12. BER performance of each layer of a 4-layer LACO-OFDM system invoking 16QAM on all of its layers communicating in AWGN channels with 8-iteration turbo code, and each layer having the same interleaver length.

[12] J. Armstrong and A. Lowery, "Power efficient optical OFDM," *Electron. Lett.*, vol. 42, pp. 370–372, Mar. 2006.

[13] Q. Wang, C. Qian, X. Guo, Z. Wang, D. G. Cunningham, and I. H. White, "Layered ACO-OFDM for intensity-modulated direct-detection optical wireless transmission," *Opt. Express*, vol. 23, pp. 12382–12393, May 2015.

[14] A. Goldsmith, *Wireless Communications*. New York: Cambridge University Press, 1 ed., 2005.

[15] H. Elgala and T. D. C. Little, "SEE-OFDM: Spectral and energy efficient OFDM for optical IM/DD systems," in *2014 IEEE 25th Annual International Symposium on Personal, Indoor, and Mobile Radio Communication (PIMRC)*, (Washington, DC, USA), pp. 851–855, Sep. 2014.

[16] E. Lam, S. K. Wilson, H. Elgala, and T. D. C. Little, "Spectrally and energy efficient OFDM (SEE-OFDM) for intensity modulated optical wireless systems," *ArXiv e-prints*, vol. abs/1510.08172, Oct. 2015.

[17] M. S. Islim, D. Tsonev, and H. Haas, "On the superposition modulation for OFDM-based optical wireless communication," in *2015 IEEE Global Conference on Signal and Information Processing (GlobalSIP)*, (Orlando, FL, USA), pp. 1022–1026, Dec. 2015.

[18] A. J. Lowery, "Enhanced asymmetrically clipped optical ODFM for high spectral efficiency and sensitivity," in *2016 Optical Fiber Communications Conference and Exhibition (OFC)*, (Anaheim, CA, USA), pp. 1–3, Mar. 2016.

[19] X. Zhang, Q. Wang, R. Zhang, S. Chen, and L. Hanzo, "Performance analysis of layered ACO-OFDM," *IEEE Access*, vol. 5, pp. 18366–18381, 2017.

[20] Q. Wang, Z. Wang, X. Guo, and L. Dai, "Improved receiver design for layered ACO-OFDM in optical wireless communications," *IEEE Photonics Technol. Lett.*, vol. 28, pp. 319–322, Feb. 2016.

[21] T. Q. Wang, H. Li, and X. Huang, "Diversity combining for layered asymmetrically clipped optical OFDM using soft successive interference cancellation," *IEEE Commun. Lett.*, vol. 21, pp. 1309–1312, Jun. 2017.

[22] M. A. Mohammed, C. He, and J. Armstrong, "Diversity combining in layered asymmetrically clipped optical OFDM," *J. Light. Technol.*, vol. 35, pp. 2078–2085, Jun. 2017.

[23] J. B. Carruthers and J. M. Kahn, "Modeling of nodirected wireless infrared channels," *IEEE Trans. Commun.*, vol. 45, pp. 1260–1268, Oct. 1997.

[24] R. Mesleh, H. Elgala, and H. Haas, "Performance analysis of indoor OFDM optical wireless communication systems," in *Proc. 2012 IEEE Wirel. Commun. Netw. Conf.*, (Paris, France), pp. 1005–1010, Apr. 2012.

[25] Y. Sun, F. Yang, and J. Gao, "Comparison of hybrid optical modulation schemes for visible light communication," *IEEE Photonics J.*, vol. 9, pp. 1–13, Jun. 2017.

[26] X. Li, J. Vucic, V. Jungnickel, and J. Armstrong, "On the capacity of intensity-modulated direct-detection systems and the information rate of ACO-OFDM for indoor optical wireless applications," *IEEE Trans. Commun.*, vol. 60, pp. 799–809, Mar. 2012.

[27] C. E. Shannon, "A mathematical theory of communication," *Bell Syst. Tech. J.*, vol. 27, pp. 379–423, Jul. 1948.

[28] R. You and J. M. Kahn, "Upper-bounding the capacity of optical IM/DD channels with multiple-subcarrier modulation and fixed bias using trigonometric moment space method," *IEEE Trans. Inf. Theory*, vol. 48, pp. 514–523, Feb. 2002.

[29] S. Hranilovic and F. R. Kschischang, "Capacity bounds for power- and band-limited optical intensity channels corrupted by Gaussian noise," *IEEE Trans. Inf. Theory*, vol. 50, pp. 784–795, May 2004.

[30] A. Chaaban, J.-M. Morvan, and M.-S. Alouini, "Free-space optical communications: Capacity bounds, approximations, and a new sphere-packing perspective," *IEEE Trans. Commun.*, vol. 64, pp. 1176–1191, Mar. 2016.

[31] A. Chaaban, Z. Rezki, and M.-S. Alouini, "Fundamental limits of parallel optical wireless channels: Capacity results and outage formulation," *IEEE Trans. Commun.*, vol. 65, pp. 296–311, Jan. 2017.

[32] J. Zhou and W. Zhang, "On the capacity of bandlimited optical intensity channels with Gaussian noise," *IEEE Trans. Commun.*, vol. 65, pp. 2481–2493, Jun. 2017.

[33] J. Zhou and W. Zhang, "A comparative study of unipolar OFDM schemes in Gaussian optical intensity channel," *IEEE Trans. Commun.*, vol. 66, pp. 1549–1564, Apr. 2018.

[34] L. Hanzo, T. H. Liew, B. L. Yeap, R. Y. S. Tee, and S. X. Ng, *Turbo coding, turbo equalisation and space-time coding: EXIT-chart-aided near-capacity designs for wireless channels*. Chichester: Wiley-IEEE Press, 2011.

[35] J. Kliewer, S. X. Ng, and L. Hanzo, "Efficient computation of EXIT functions for nonbinary iterative decoding," *IEEE Trans. Commun.*, vol. 54, pp. 2133–2136, Dec. 2006.

[36] Z. Babar, S. X. Ng, and L. Hanzo, "Near-capacity code design for entanglement-assisted classical communication over quantum depolarizing channels," *IEEE Trans. Commun.*, vol. 61, pp. 4801–4807, Dec. 2013.

[37] T. M. Cover and J. A. Thomas, *Elements of information theory*. Hoboken, New Jersey: John Wiley & Sons, 2 ed., 2012.

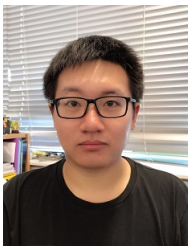

Xiaoyu Zhang (S'16) received the B.Eng. degree in electronic information engineering from University of Electronic Science and Technology of China (UESTC), and the MSc degree with Distinction from University of Southampton, UK. Currently he is working towards the PhD degree with Next Generation Wireless Group, University of Southampton. His research interests lie in the areas of full-duplex communications and visible light communications.

Zunaira Babar received her B.Eng. degree in electrical engineering from the National University of Science & Technology (NUST), Islamabad, Pakistan, in 2008, and the M.Sc. degree (Distinction) and the Ph.D degree in wireless communications from the University of Southampton, UK, in 2011 and 2015, respectively. She is currently working as a Research Fellow in the Next Generation Wireless group, University of Southampton. She is the recipient of several academic awards, including the Commonwealth Scholarship by the Government of UK (2010-2011) and the Dean's Award for Early Career Research Excellence by the University of Southampton (2018). Her research interests include classical and quantum error correction codes, coded modulation, joint source and channel coding, error reconciliation for quantum key distribution, quantum-assisted communications and optical communications.

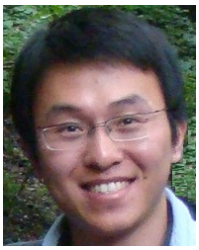

Rong Zhang (M'09-SM'16) is an assistant professor in Southampton Wireless group within the school of ECS at University of Southampton (UoS). He received his PhD in wireless communications from UoS in 2009, where he was a research assistant during that period with Mobile Virtual Centre of Excellence, one of UK's largest industrial-academic partnership in ICT. During his post-doctoral period in ECS, he contributed as the UoS lead researcher on a number of international projects. After that, he took his industrial consulting leave for Huawei EU R&D as a System Algorithms Expert. He has a total of 90+ IEEE/OSA publications, including 60+ journals (20+ of which as first author). Owing to his outstanding academic achievements, he is the recipient of the prestigious Dean's Publication Award. He is also the recipient of the prestigious RAEng industrial fellowship. He regularly serves as editor/reviewer for IEEE/OSA journals and funding bodies and has been several times as TPC member/invited session chair of major conferences. He is a RAEng industrial fellow, a senior member of the IEEE, a member of the OSA and a member of the HEA.

Sheng Chen (M'90-SM'97-F'08) received the B.Eng. degree in control engineering from the East China Petroleum Institute, Dongying, China, in January 1982, the Ph.D. degree in control engineering from City University, London, in September 1986, and the higher doctoral degree (D.Sc.) from the University of Southampton, Southampton, U.K., in 2005. He held research and academic appointments with the University of Sheffield, the University of Edinburgh, and the University of Portsmouth, U.K., from 1986 to 1999. Since 1999, he has been with the Electronics and Computer Science Department, University of Southampton, where he is a Professor of Intelligent Systems and Signal Processing. His research interests include adaptive signal processing, wireless communications, modeling and identification of nonlinear systems, neural network and machine learning, intelligent control system design, evolutionary computation methods, and optimization. He has authored over 550 research papers. Dr. Chen is a fellow of the United Kingdom Royal Academy of Engineering, a fellow of IET, and a Distinguished Adjunct Professor with King Abdulaziz University, Jeddah, Saudi Arabia. He was an ISI Highly Cited Researcher in engineering in 2004.

Lajos Hanzo (M'91-SM'92-F'03) FREng, FIEEE, FIET, Fellow of EURASIP, DSc received his degree in electronics in 1976 and his doctorate in 1983. In 2009 he was awarded an honorary doctorate by the Technical University of Budapest and in 2015 by the University of Edinburgh. In 2016 he was admitted to the Hungarian Academy of Science. During his 40-year career in telecommunications he has held various research and academic posts in Hungary, Germany and the UK. Since 1986 he has been with the School of Electronics and Computer Science, University of Southampton, UK, where he holds the chair in telecommunications. He has successfully supervised 112 PhD students, co-authored 18 John Wiley/IEEE Press books on mobile radio communications totalling in excess of 10 000 pages, published 1776 research contributions at IEEE Xplore, acted both as TPC and General Chair of IEEE conferences, presented keynote lectures and has been awarded a number of distinctions. Currently he is directing an academic research team, working on a range of research projects in the field of wireless multimedia communications sponsored by industry, the Engineering and Physical Sciences Research Council (EPSRC) UK, the European Research Council's Advanced Fellow Grant and the Royal Society's Wolfson Research Merit Award. He is an enthusiastic supporter of industrial and academic liaison and he offers a range of industrial courses. He is also a Governor of the IEEE ComSoc and VTS. During 2008 - 2012 he was the Editor-in-Chief of the IEEE Press and a Chaired Professor also at Tsinghua University, Beijing. For further information on research in progress and associated publications please refer to http://www-mobile.ecs.soton.ac.uk